JOURNAL OF MATERIALS SCIENCE **39** (2004) 2617– 2620

SEM online investigation of fatigue crack initiation and propagation in cast magnesium alloy

XI-SHU WANG*
Department of Engineering Mechanics, Tsinghua University, Beijing 100084, People's Republic of China
E-mail: xshwang@tsinghua.edu.cn

JING-HONG FAN
Research Center on Materials Mechanics, Chongqing University, 400044, People's Republic of China; Division of Mechanical Engineering, Alfred University, NY 14802, USA

Magnesium (Mg) alloys have a unique combination of properties including low density and easy formability that are attractive for numerous technological applications. The requirement to reduce the weight of engineering components has recently triggered substantial research effort on the structural properties of this kind of alloy [1–3]. Compared to other lightweight wrought and cast materials such as aluminum and titanium, little work has been performed on the fatigue behavior of cast magnesium. Initial studies examined the low and high cycle fatigue of cast Mg [4, 5] but they concluded that traditional fatigue life prediction tools are often inaccurate for the cast Mg. Therefore, it is of great interest to search for a relationship between the fatigue failure mechanisms and microstructure in the cast Mg [6–9]. To gain a better understanding on the fatigue behaviors of this alloy, we carried out the fatigue crack initiation and propagation tests and investigated the fatigue crack growth path with notched specimens of the cast AM50 alloy with online SEM observation.

The nominal composition of AM50 alloy contain about 5 wt% aluminum. The testing specimens with a 14 mm gage length and a 2.5 mm by 2.3 mm gage cross section were machined from plates supplied by Hydro's Inc. The testing specimen had a notch radius of about $\rho = 80\ \mu$m to elevate the local stress state in controlling the site of fatigue crack initiation. The surfaces of the samples were carefully polished prior to fatigue tests. All fatigue tests were performed in the chamber of the SEM. Fatigue tests were carried out at a stress ratio $R = 0.1$ under a sinusoidal variation. The maximum stress of 120 MPa was chosen as it is below the yield stress $\sigma_{0.2} = 140$ MPa. The whole process of fatigue crack initiation and propagation was monitored and recorded in situ at a frequency of 0.01 Hz at room temperature in order to clearly observe the open and closed crack status. The microstructure of cast AM50 alloy is present in the brittle eutectic phase $Mg_{17}Al_{12}$ (Its micro-hardness is about 88.34 MPa) with the α-Mg grains (Its micro-hardness is about 66.86 MPa). The microstructure has a significant influence on the mechanical properties of this alloy [10]. As tensile fracture initiates due to cracking of $Mg_{17}Al_{12}$ particles [11], the volume fraction and spatial distribution of this β-phase determines the ductility, provided that there are no severe defects such as porosity or oxide films.

Fig. 1 shows the S-N curve of cast AM50 alloy with a notch. With increasing applied stress, the fatigue failure life N_f decreases linearly in the range from 2×10^3 to 10^6. When the applied maximum stress is near to the yield stress, the fatigue bifurcate crack along the grains boundaries of the primary α-Mg globules was found, as shown in Fig. 2. In the later stage after a bifurcate crack occurs, the fatigue crack growth life is much lower than the fatigue crack initiation life if the fatigue life is defined as the summation of loading cycles of the above-mentioned two regimes. This means that the fatigue crack initiation life is approximately equal to the total fatigue life of the alloy because it is significantly affected by the microstructure as well as the shape and size of notch of samples. Therefore, one should pay special attention to the effect of microstructure on the fatigue crack initiation of the alloy. As the ductility of boundary of α-Mg grains is rather lower, the fatigue behavior of this alloy is not excellent. Therefore, the ductility should be enhanced by a decrease in the volume fraction of the β-phase as well as by a finer dispersion of the β-phase so as to form a continuous network of the β-phase along the grain boundary α-Mg globules. Micromechanical analysis shows that the continuous network microstructure of the β-phase may provide superior stiffening and strengthening effects to the alloy [12].

When the maximum applied stress reached 120 MPa ($\sigma_{max}/\sigma_{0.2} \leq 0.857$), the early fatigue crack propagation path after 82 657 cycles was shown in Fig. 3a and b. The fatigue crack initiation shown in Fig. 3a also shown that the fatigue crack initiation depend mainly on the microstructure of material no matter under a higher or lower stress level. It is clearly seen that the crack initiated at location A which was not located at the tip of notch and a *V*-shape fatigue crack propagation path formed at the early stage of the crack growth.

*Author to whom all correspondence should be addressed.

0022–2461

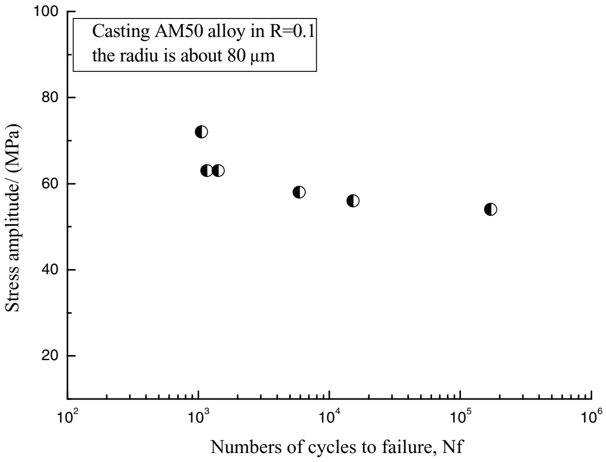

Figure 1 S-N curve for cast AM50 alloy.

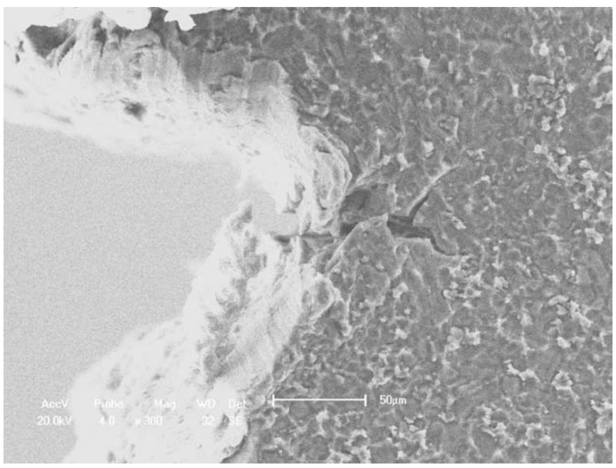

Figure 2 Fatigue crack initiation and propagation path under applied maximum stress 160 MPa at $R = 0.1$ (scale bar 50 μm).

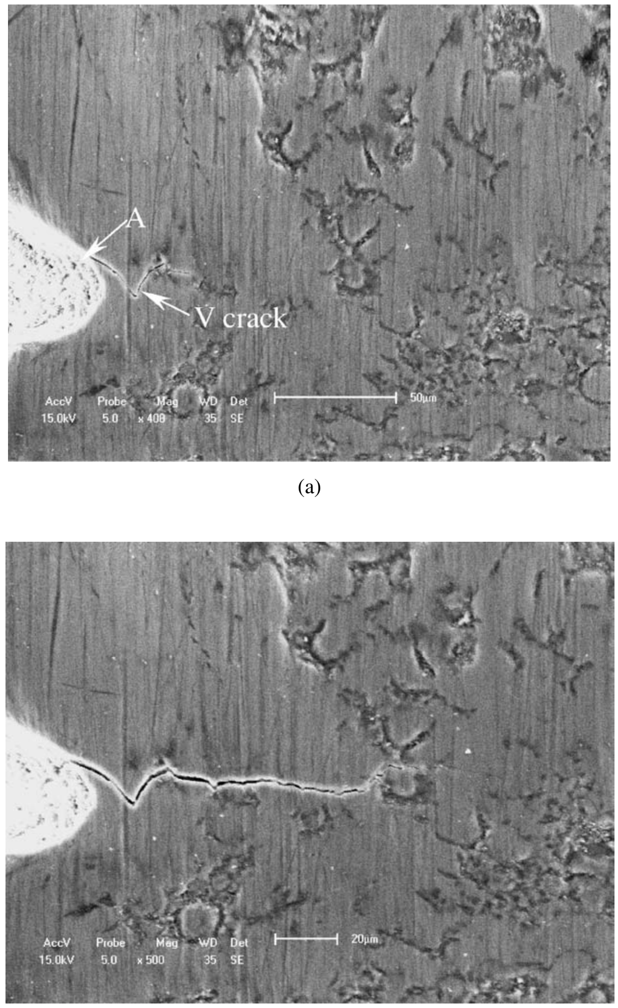

(a)

(b)

Figure 3 Fatigue crack initiation and propagation path under applied maximum stress 120 MPa at $R = 0.1$. (a) Fatigue microcrack propagation path after $N = 82\,657$ (scale bar 50 μm, $\ell = 42$ μm). (b) Fatigue microcrack propagation path after $N = 140\,639$ (scale bar 20 μm, $\ell = 134$ μm).

The crack completed the transition from the *V*-type to mode-I type crack after 140 639 cycles of loading, corresponding to a crack length about 134 μm. Thus the crack changed its propagation direction from the inclined direction to the straight one, i.e., perpendicular to the loading direction. This rotation of propagation direction was caused mainly by the increase of driving force (stress intensity factor) due to the increase of crack length and the effect of the microstructure of material. When the crack growth approached to a location, where dense β-$Mg_{17}Al_{12}$ phase in the multiple α-Mg grains boundaries were distributed, the rotation of crack propagation direction occurred. Due to the micro-hardness of the β-$Mg_{17}Al_{12}$ phase is much higher, when the cyclic plastic zone in front of the crack tip had a sufficient size to include this region, these brittle β-$Mg_{17}Al_{12}$ phase has a great influence on mechanical properties resulting in the sliding of grain boundary. This will facilitate the crack propagation so the crack will switch from Mode-I type and propagate along a locally curved path along the α-Mg grains boundaries.

Fig. 4a shows a SEM image of the microstructure of the alloy on the fracture surface. Here, it can be seen that the geometry of the upper surfaces of phases 1 and 2 formed a *V*-shape. There is a third phase between phases 1 and 2, but is not shown in this figure as only the fracture part was observed. To verify that these phases are the primary α-Mg phase, local chemical compositions were determined using Energy Dispersive X-ray (EDX) analysis. Results showed that the Mg contents of phases 1 and 2 are, respectively, 88.4 and 90.9%; see Fig. 4b and c. From this composition characterization, we can conclude that the crack passed through the α-Mg grains boundaries.

In summary, we obtain the following main conclusions from this study. (a) Fatigue cracks were observed to nucleate preferentially in porous notched regions, especially at the site with a high stress concentration. (b) Fatigue crack initiation and propagation behavior can be improved by the ductility which changes with the cast process. (c) The Mode-I small crack propagation can be disturbed by interdendritic regions where the harder β-phase requires a higher stress to cause debonding from the α-phase which has a lower resistance for crack propagation.

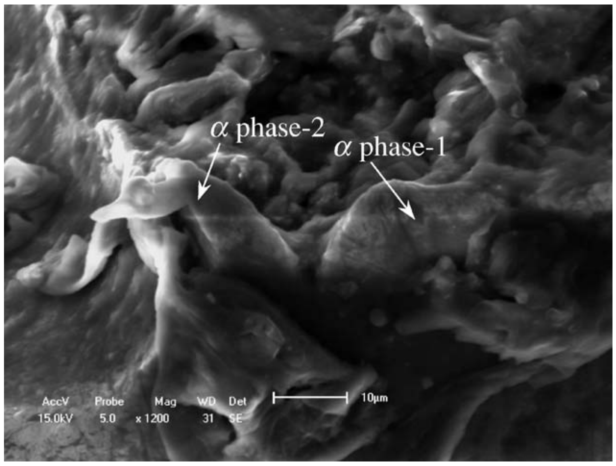

(a)

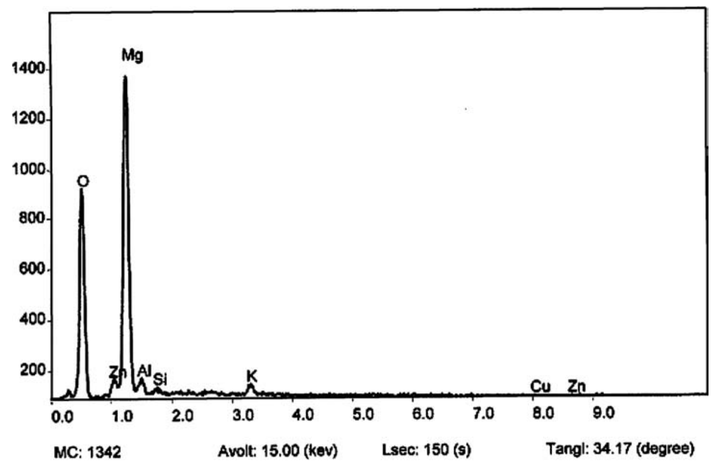

Quantity Result

Element	Weight%	Atomic%	Net Inten	ZAF Corr	Series
Mg	88.44	90.30	12700	0.97	K
Al	7.83	7.21	470	0.40	K
Si	2.13	1.89	158	0.50	K
Zn	1.60	0.61	11	0.58	K

(b)

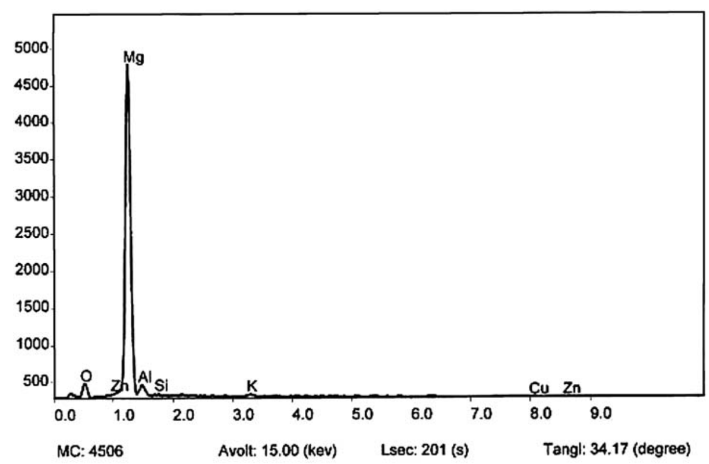

Quantity Result

Element	Weight%	Atomic%	Net Inten	ZAF Corr	Series
Mg	90.90	91.75	47215	1.00	K
Al	8.23	7.48	1708	0.40	K
Si	0.87	0.76	223	0.49	K
Zn	0.00	0.00	0	0.00	K

(c)

Figure 4 SEM image of the surface microstructure and chemical composition of material: (a) SEM image of the surface microstructure of material (scale bar 10 μm), (b) the chemical composition of Mg α-phase 1 via EDX, and (c) the chemical composition of Mg α-phase 2 via EDX.

Acknowledgments
The authors would like to thank the financial support of USCAR/VSamp and Richard J. Osborne and Donald E. Penrod for significant support of this project.

References

1. B. L. MORDIKE and T. EBERT, *J. Mater. Sci. Engng.* A**302** (2001) 37.
2. M. M. AVEDASIAN and H. BAKER, "ASM Specialty Hand Book" (ASM International, Ohio, 1999).
3. S. KLEINER, O. BEFFORT, A. WAHLEM and P. J. UGGOWITZER, *J. Light Metals* **2** (2002) 277.
4. D. L. GOODENBERGER and R. I. STEPHENS, *J. Engng. Mater. Techn.* **115** (1993) 391.
5. G. EISENMEIER, M. OTTMUELLER, H. W. HOEPPEL and H. MUGHRABI, in Fatigue'99, Proceedings of the 7th International Fatigue Conference (Beijing, P.R. China, 1999) Vols. 1/4, p. 253.
6. A. BALASUNDARAM and A. M. GOKHALE, *Mater. Character.* **46** (2001) 419.
7. A. M. GOKHALE and G. R. PATEL, in "Magn. Techn.," edited by J. Hryn (TMS, 2001) p. 195.
8. A. K. DAHLE, Y. C. LEE, M. D. NAVE, P. L. SCHAFFER and D. H. STJOHN. *J. Light Metals* **1** (2001) 161.
9. K. XU, A. M. RUSSELL, L. S. CHUMBLEY and F. C. LAABS, *J. Mater. Sci.* **34**(24) (1999) 5955.
10. D. J. SAKKINEN, "Attributes of Magnesium for Automobile Design" (SAE, Warrendale, 1994) p. 71.
11. G. L. DUNLOP, W. P. SEQUEIRA, M. S. DARGUSCH, G. SONG, A. ATRENS, T. KITTEL, D. H. STJOHN, A. K. DAHLE and M. MURRAY, in Proceedings of The 55th Meeting of The International Magnesium Association, 1998, p. 68.
12. X. Q. FENG, Y.-W. MAI and Q. H. QIN, *Comput. Mater. Sci.* (in press).

Received 10 February and accepted 26 September 2003